Secondary current effects on cohesive river bank erosion

Athanasios N. Papanicolaou,[1] Mohamed Elhakeem,[1] and Robert Hilldale[2]

Received 23 November 2006; revised 15 August 2007; accepted 20 September 2007; published 29 December 2007.

[1] The emphasis of this research was placed on the development of a methodology that allows (1) an adequate representation of the distribution of the near-bank shear stress τ_s when secondary currents are present and (2) estimation of the critical erosional strength τ_{cr} and other sediment erodibility parameters for fluvial erosion. These two factors combine to form the overarching objective of this investigation, which was carried out in Union Flat Creek, a stream with pronounced cross-sectional irregularities located within the loess region of the Palouse basin of Washington State, United States. The study has shown that the presence of the secondary currents increases the magnitude of the depth-averaged sidewall shear stress at least by a factor of 2.0. It was also found that the ratio of the maximum to the depth-averaged sidewall shear stress $\bar{\tau}_s$ is greater than 5. These findings suggest therefore that use of the $\bar{\tau}_s$ may be a good approximation of the fluid shear stress magnitude for simple channel geometries but not for natural channels characterized by complex geometries. The measured critical erosional strength (τ_{cr} = 4.16 Pa) was comparable with the findings of other laboratory and field studies that also focused on Palouse sediments.

Citation: Papanicolaou, A. N., M. Elhakeem, and R. Hilldale (2007), Secondary current effects on cohesive river bank erosion, *Water Resour. Res.*, *43*, W12418, doi:10.1029/2006WR005763.

1. Introduction

[2] Different models are available to calculate the sidewall shear stress exerted on a bank. Most of the models assume uniform flow conditions and consider a near-bank shear stress distribution derived from laboratory experiments [e.g., *Leutheusser*, 1963; *Kartha and Leutheusser*, 1970; *Simons and Senturk*, 1992; *Knight et al.*, 1984; *Flintham and Carling*, 1988; *Millar and Quick*, 1998] or analytically [*Duan*, 2005]. However, these assumptions should only be applied with caution to natural rivers, as the simple channel geometries investigated in flumes represent the flow-bank interaction rather poorly.

[3] Natural rivers are characterized by complex geometries such as channel expansions and contractions, bends, and variable bed and bank roughness. These features are believed to create an unbalanced turbulent stress distribution along the cross-sectional plane, thus leading to the formation of secondary currents [*Nezu et al.*, 1993; *Ervine et al.*, 2000; *van Prooijen et al.*, 2005]. It is therefore important to account for the effects of secondary currents on a flow field to provide accurate estimates of the applied sidewall shear stress (τ_s) distribution on a river bank. Another limitation that most of the models possess is that their predictions are provided in terms of an averaged sidewall shear stress, $\bar{\tau}_s$ instead of a τ_s distribution. Studies by *Kean and Smith* [2006a, 2006b] have shown that τ_s is highly variable both in space and time, and is dependent on many factors such as channel planform, geometry and flow stage [*Couper*, 2003, 2004]. This variability presents a challenge for anyone seeking to characterize the sidewall shear stress distribution exerted on a bank, for bank erosion studies, by means of analytical methods and/or direct measurements [e.g., *Hanson*, 1990; *Hanson and Simon*, 2001; *Kean and Smith*, 2006a, 2006b].

[4] Bank erosion of cohesive sediments occurs as mass failure or fluvial (hydraulic) erosion. Mass failure is associated with the sediment's mechanical strength and is defined as the collapse of the bank material when critical height and angle have been exceeded. Mass failure often occurs at discrete instances during a discharge hydrograph. Conversely, fluvial erosion of cohesive banks is associated with the particle-by-particle erosion and can take place daily over a period of months. Fluvial (or equivalently hydraulic) erosion is defined here as the entrainment or dislodgement of individual cohesive particles or aggregates at the flow-sediment interface because of the flow shearing action [e.g., *Knighton*, 1973]. Fluvial erosion commences when the sidewall shear stress (τ_s) applied by the flow to the bank surface exceeds a surrogate measure of cohesion, known as the critical erosional strength (τ_{cr}). The critical erosional strength denotes the cohesion strength provided by interparticle forces of attraction or repulsion acting at the microscopic level, including electrostatic forces, van der Waals forces, hydration forces and biological forces. A number of excellent reviews [e.g., *Thorne and Tovey*, 1981; *Grissinger*, 1982; *Thorne*, 1982; *Kamphuis and Hall*, 1983; *Thorne*, 1990; *Lawler*, 1993; *Lawler et al.*, 1997; *Abernethy and Rutherford*, 1998; *ASCE Task Committee on Hydraulics, Bank Mechanics, and Modeling of River Width Adjustment*, 1998; *Simon et al.*, 2000; *Simon and Rinaldi*, 2000; *Rinaldi and Darby*, 2005; *Pizzuto et al.*, 2007] reveal that very little attention has been placed on

[1]Department of Civil and Environmental Engineering, IIHR-Hydroscience and Engineering, University of Iowa, Iowa City, Iowa, USA.
[2]Sedimentation and River Hydraulics Group, Technical Service Center, Bureau of Reclamation, Denver, Colorado, USA.

0043-1397/07/2006WR005763

Figure 1. Union Flat Creek in Washington State, United States. (a) Reed canary grass (*Phalaris arundinacia*) on the upper and lower banks of the channel. The upper bank is only visible in the top left corner of the picture. (b) Side view of a typical upper bank in Union Flat Creek.

fluvial erosion of cohesive river banks compared to mass failure.

[5] The emphasis of this research was placed on the development of a methodology that allows (1) an adequate representation of the distribution of the near-bank shear stress τ_s when secondary currents are present and (2) estimation of the critical erosional strength τ_{cr} and other sediment erodibility parameters for fluvial erosion. These

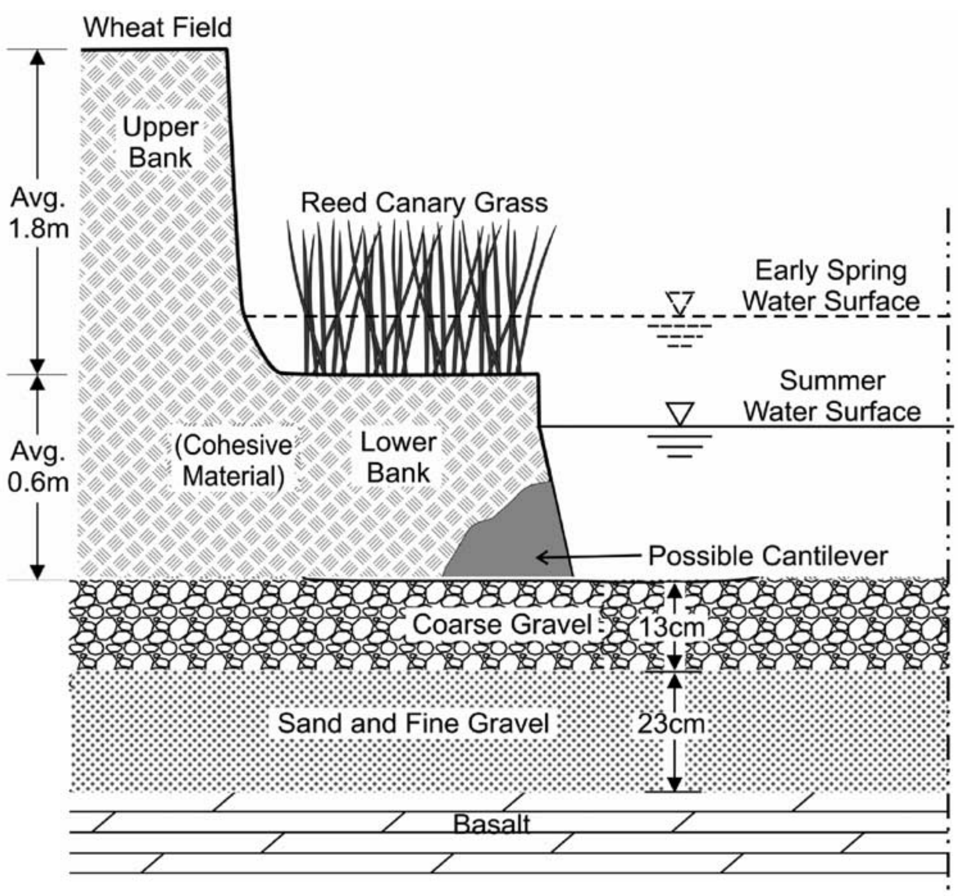

Figure 2. Typical cross section of the Union Flat Creek showing the bed material of the lower bank and substrate. Depths shown are the average for the reach studied and were determined with a hand-held cone penetrometer.

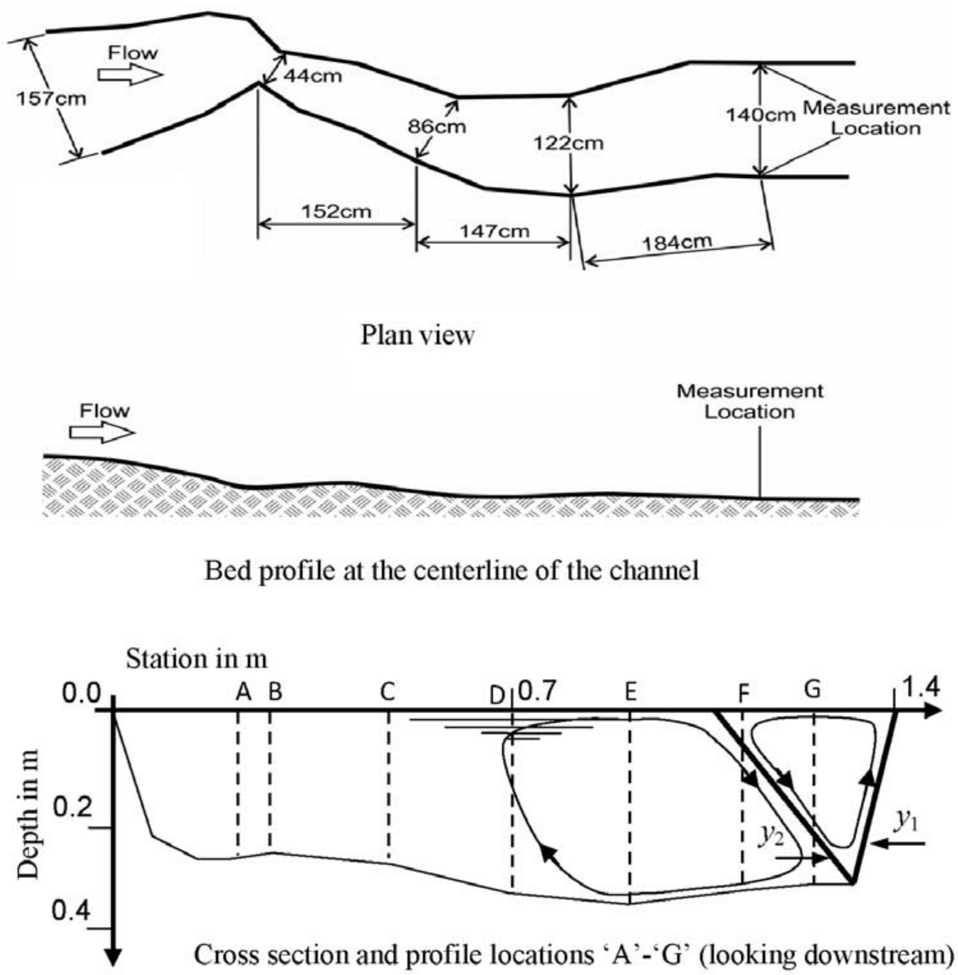

Figure 3. Geometry of the studied reach of Union Flat Creek. Of particular interest is the contraction to a width of 0.44 m and the subsequent gradual expansion to a width of 1.4 m at the measurement location (plan view). The cross-section view shows the location of vertical profiles in which velocity data were taken. References to left and right bank are consistent with this diagram (left bank near vertical A). The apex bend is located approximately 3.0 m upstream of the measurement location. The radius of curvature of the bend was 5.0 m, and the arc angle was 49°.

two factors combine to form the overarching objective of this investigation, which was carried out in Union Flat Creek, located within the loess region of the Palouse basin of Washington State, United States.

2. Goals and Study Design

[6] The first goal of this research was to quantify the effects of secondary currents on the sidewall shear stress τ_s. For this purpose, a preliminary investigation was carried out to carefully select the flow event and location suitable for detailed flow measurements of turbulence and secondary velocities. The investigation concluded that 3 July of 2000 is an adequate time for the acquisition of the flow measurements via an acoustic Doppler velocimeter (ADV), when the discharge of Union Flat Creek did not fluctuate more than 3% throughout the day.

[7] The second goal of this study was to develop the methodological steps for determining the onset of fluvial erosion for the cohesive bank sediments of Union Flat. We have selected to demonstrate the fluvial erosion methodology for the 3 July event for two reasons. The first reason was that we had a priori knowledge of the sidewall stress for that event via the detailed ADV flow measurements (first goal of the study). Second, the role of the freeze and thaw, active floodplains, and pore pressure fluctuations on the critical erosional strength during the summer period in the upper part of the Palouse watershed was minimal [*McCool et al.*, 2000]. In addition, no desiccation was reported in the upper part of the Palouse watershed for the period of our measurements [*Mancilla*, 2004]. The field component of the study in Palouse involved the installation of erosion pins, and optical backscatter sensors (OBS) to measure fluvial erosion for the 3 July flow event. In addition, laboratory experiments were performed on undisturbed samples of the bank sediment to determine the critical erodibility parameters for Union Flat Creek. A new flume design was proposed to facilitate fluvial erosion experiments of undisturbed sediments samples under controlled laboratory conditions. More details about the flow and erosion

Table 1. Summary of Flow Parameters and Cross-Section Geometry in Union Flat Creek During Measurements[a]

Condition	Value
Q, m^3/s	0.10
V, m/s	0.27
S	3.74×10^{-4}
W, m	1.28
D, m	0.29
R_e	2×10^5
F_r	0.16
W/D	4.4

[a]Conditions during measurements are the volumetric discharge Q; the mean velocity V defined as $Q/(WD)'$ the Reynolds number R_e defined as the ratio $(4R\ V)/\nu$; the Froude number F_r defined as the ratio $V/(gH)^{1/2}$; and the ratio W/D, where W and D denotes the average cross-sectional width and depth, respectively, g denotes the gravitational acceleration, R denotes the hydraulic radius, and ν denotes the kinematic viscosity.

measurements in the field and laboratory are provided in section 4.

3. Study Area

[8] Union Flat Creek is a gravel bed channel with cohesive banks that flows through the Upper Palouse watershed in the semiarid region of eastern Washington State, United States [*Northwest Power Planning Council*, 2001]. The stream has pronounced cross-sectional irregularities, described by a sequence of channel expansions and contractions along its length and was ideal for studying the effects of secondary effects on cohesive bank erosion (Figure 1). Figure 2 shows a typical cross section of Union Flat Creek, which typically exhibits an upper and lower bank. The studied reach and the measurement location were located at an expansion which was 4.8 m (approximately 3.5 channel widths) downstream from the constricted point of the channel (Figure 3).

4. Methodology

4.1. Flow Component

4.1.1. Theoretical Analysis

[9] To account for the contributions of secondary flows and turbulence on sidewall shear stress, the Reynolds equation in the streamwise direction, x, was considered:

$$\bar{v}\frac{\partial \bar{u}}{\partial y} + \bar{w}\frac{\partial \bar{u}}{\partial z} = gS + \frac{1}{\rho}\left(\frac{\partial \tau_{yx}}{\partial y} + \frac{\partial \tau_{zx}}{\partial z}\right) \quad (1)$$

where ρ is the fluid density (kg/m3), g is gravitational acceleration (m/s2), S is the channel slope, $\bar{u}$, $\bar{v}$ and $\bar{w}$ denote the time average velocities (m/s) in the x, y and z directions respectively, and τ_{zx} and τ_{yx} are shear stresses (Pa) in the streamwise direction, x, applied on the z-x plane and the y-x plane, respectively. By integrating equation (1) in the transverse direction, y, the following equation is obtained:

$$\frac{\tau_{yx}}{\rho} = \underbrace{\int_{y_1}^{y_2} gSdy}_{A} + \underbrace{\int_{y_1}^{y_2} \partial\bar{u}\,\bar{v}}_{B} + \underbrace{\int_{y_1}^{y_2} \frac{\partial \bar{u}\,\bar{w}}{\partial z}dy}_{C} - \underbrace{\int_{y_1}^{y_2} \frac{\partial}{\partial z}\left(\frac{\tau_{zx}}{\rho}\right)dy}_{D} \quad (2)$$

The integral limits y_1 and y_2 describe the bank line geometry of the channel and the line separating the core flow of the channel from the flow contributing to the sidewall shear stress, respectively (Figure 3). y_2 is defined in the literature as the demarcation line between the core flow and the recirculating region [*Guo and Julien*, 2005].

[10] In equation (2) term A accounts for gravity, terms B and C account for secondary flow effects and D accounts for the Reynolds stress contributions. To determine the sidewall shear stress (τ_s) distribution along the bank wall, equation (2) was modified by setting $gS = u_*^2/R$ and $\bar{v} = 0$ along y_1 at the bank boundary. The modified equation was written as follows:

$$\frac{\tau_s}{\rho} = \int_{y_1}^{y_2} \frac{u_*^2}{R}dy - \frac{\partial}{\partial z}\int_{y_1}^{y_2} \left(\bar{u}\ \bar{w} + \overline{u'w'}\right)dy \quad (3)$$

where u_* is the friction velocity at the sidewall (m/s) and R is the hydraulic radius (m). The term $(\bar{u}\ \bar{w} + \overline{u'w'})$ in the right side of equation (3) denotes the total momentum flux that is exchanged across the channel cross-sectional plane (between the core flow and sidewall contributing areas) because of the secondary velocity $\bar{w}$ and the fluctuating term $\overline{u'w'}$. Equation (3) suggests that the τ_s distribution (shape and magnitude) was affected by the gravitational contributions and the rate of the momentum flux along the vertical direction z that is exchanged between the core of the flow and the near-bank area. The steps involved in determining the τ_s distribution by using direct flow measurements are provided in subsequent sections.

4.1.2. Flow Measurements

[11] The flow discharge at the measurement location on 3 July 2000 was measured following USGS procedures [*Corbett*, 1962]. Table 1 provides a summary of the flow parameters and cross-sectional geometry in Union Flat Creek.

[12] Seven velocity profiles were taken at the cross section for mapping the flow field and determine the terms in equation (3). The measurements were conducted with a SonTek ADV (10 MHz) with 155 measuring points across the cross section (Figure 3). Wall effects extended typically at about 15% of the channel width away from the bank and toward the centerline. For this reason, no measurements were made within that distance away from the bank as the quality of the ADV signal was poor (rejection rate was higher than 60%). The ADV was mounted to a 5.0 cm square steel tubing that was attached to a scaffold spanning the channel width so it did not disturb the flow field. By mounting the probe to a rigid scaffold, any possible vibration of the probe due to flow action was minimized.

Table 2. Properties of Bank Sediment in Union Flat Creek

Property	Value
LL	41.9
PL	33.0
Percent $WC_{natural}$	55
ϕ, deg	37.8
SG	2.68
ρ_{bulk}, kg/m^3	1350

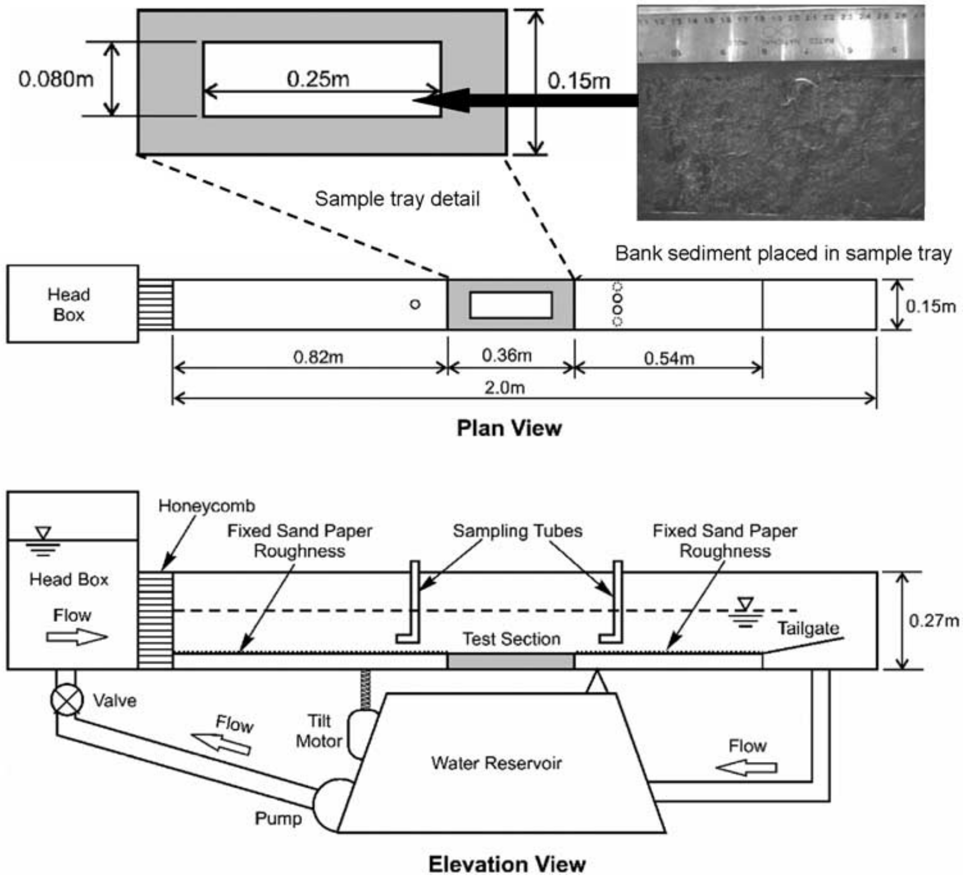

Figure 4. Laboratory flume equipped with a sediment box sampler for testing critical erosional strength. Shown at top right is a bank sediment sample placed in the box sampler for testing its critical erosional strength.

[13] The ADV sampling volume (approximately 0.25 cm^3) was located 5.0 cm from the transmitting transducer. This enabled the collection of turbulence measurements without interfering with the flow. Data points in each profile were vertically spaced at 1.0 cm with the exception of the three points closest to the bed, which were spaced at 0.5 cm to better define the near-wall region. This detailed mapping of the flow was necessary for determining the terms in equation (3). For the first three points of each vertical profile, 3,000 samples were collected while the remaining points were sampled 1,500 times. Depth was periodically measured throughout the data collection process to ensure constant flow conditions. The data were filtered to remove signal noise. Filter criteria for the data was set to reject average correlation values less than 70% (recommended by

Table 3. Experimental Conditions for the Flume Critical Fluvial Erosion Tests[a]

Experiment	$Q \times 10^{-3}$, m^3/s	V, m/s	R, m	S	τ, Pa	R_e	$R_o \times 10^4$	W/D	$(C_s)_{up}$, mg/L	$(C_s)_{down}$, mg/L	ΔC_s, mg/L	$E \times 10^5$, $kg/m^2/s$
E-1	2.615	0.830	0.021	0.020	4.116	10476	4.66	7.1	63	63.0	0.0	0.000
E-2	2.942	0.864	0.023	0.020	4.449	11583	4.83	6.6	68	68.1	0.1	0.147
E-3	3.219	0.933	0.023	0.023	5.184	12632	5.06	6.5	71	71.0	0.0	0.000
E-4	2.981	0.946	0.021	0.026	5.351	11944	5.59	7.1	72	72.2	0.2	0.298
E-5	3.870	0.992	0.026	0.023	5.860	14736	5.63	5.8	83	86.0	3.0	5.800
E-6	4.110	1.055	0.026	0.026	6.625	15668	6.20	5.8	89	92.0	3.0	6.170
E-7	4.270	1.095	0.026	0.028	7.134	16259	6.39	5.8	91	93.8	2.8	5.980
E-8	4.345	1.114	0.026	0.029	7.389	16547	6.48	5.8	92	96.8	4.8	10.400
E-9	4.624	1.199	0.026	0.034	8.563	17661	7.04	5.8	97	100.4	3.4	7.860
E-10	4.841	1.218	0.027	0.034	8.830	18343	6.86	5.7	97	101.5	4.5	10.900
E-11	5.310	1.255	0.028	0.034	9.396	19790	6.96	5.3	102	107.1	5.1	13.500
E-12	8.217	1.442	0.038	0.034	12.662	27969	6.99	3.9	123	127.6	4.6	18.900

[a]The first eight columns provide the conditions during the fluvial erosion runs. These are the volumetric discharge Q; the mean velocity V; the hydraulic radius R; the gradient S; the applied shear stress $\tau = \gamma R S$; the Reynolds number R_e; the Rouse number $R_o = w_s/(\kappa u_*)$, where $\kappa = 0.41$ and w_s is the average fall velocity of the sediment particles related to the concentration of sediment in the water C_s by $w_s = 1.34 \times 10^{-4}\ C_s^{137}$ [*Burt and Stevenson*, 1983]; and the ratio (W/D).

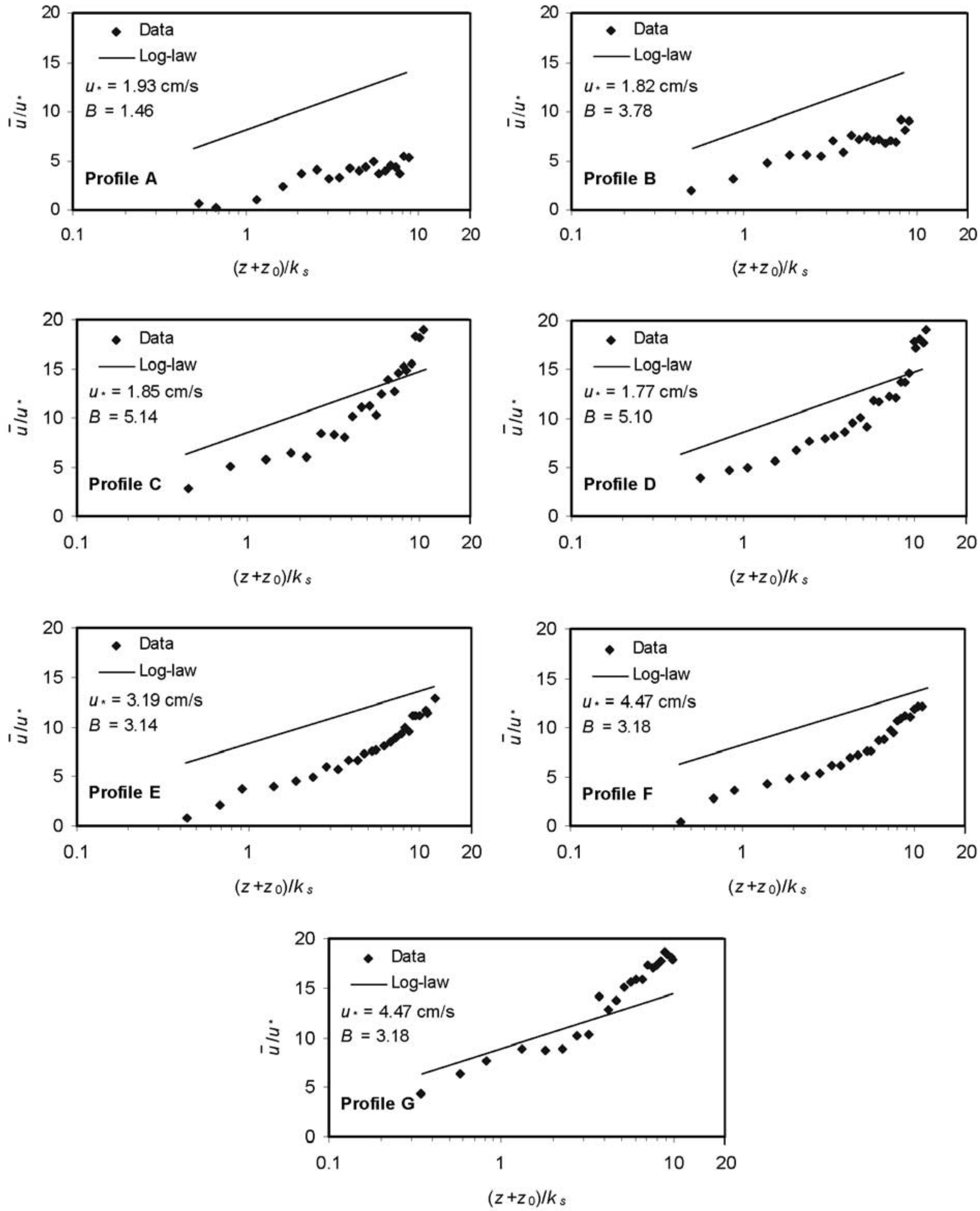

Figure 5. Velocity profiles for locations A–G. The solid line is the log law (equation (5), with $B = 8.5$), and the diamonds represent point-averaged velocity.

SonTek). In all but a few isolated cases, rejection was less than 10%, most being less than 5%.

4.2. Bank Sediment Erosion Component

4.2.1. Field Component and Sediment Analysis

[14] The study location was surveyed prior and after the flow measurements to mark the changes occurring in the bank line. In addition, two OBSs (model 3) were placed downstream and upstream from the study location for recording suspended sediment on a continuous basis for the duration of the field experiment on 3 July 2000. Lastly, erosion pins were placed along the lower bank. The exposed length of the pins was recorded at the end of the flow measurements.

Table 4. Frictional Characteristics of the Flow in Union Flat Creek[a]

Profiles	H, m	U, m/s	u_*, m/s	B (equation (5))	ΔB (equation (5))
A	0.179	0.079	0.0193	1.46	7.01
B	0.183	0.126	0.0182	3.78	4.69
C	0.211	0.227	0.0185	5.14	3.33
D	0.237	0.220	0.0177	5.10	3.37
E	0.254	0.287	0.0319	3.14	5.33
F	0.224	0.393	0.0447	3.18	5.29
G	0.202	0.417	0.0275	7.56	0.91

[a]The friction velocity was estimated via the Clauser method applied to the inner region ($z/H < 0.2$). B denotes the constant of integration for equation (5). ΔB values are a shift from the published B averaged value of 8.47 [*Kironoto and Graf*, 1994].

[15] Sediment samples were extracted from a bank toe located downstream of the channel cross section where the measurements were taken to prevent alteration of the flow field. The pH of the stream water where the samples were stored was 8.2 and the temperature of the stream water was 17–18°C. All samples were extracted from the bank toe by using the same procedure and remained saturated in their native river water during transportation.

[16] The average values for the physical properties of the bank sediment such as the plastic limit (*PL*), liquid limit (*LL*), the natural water content (WC_{natural}), friction angle (ϕ), specific gravity (*SG*) and in situ bulk density (ρ_{bulk}) are given in Table 2. These properties were obtained using the procedures outlined by *Papanicolaou* [2001]. According to the Unified Classification System plasticity chart for the determined *PL* and *LL*, the bank sediment in Union Flat Creek was classified as *ML* (silt of low plasticity).

[17] The bank sediment composition of Union Flat Creek is 60% sand, 27% silt and 13% clay with a median grain size diameter of 0.08 mm. The bank sediment in Union Flat Creek was determined to contain about 1% organic carbon [*Papanicolaou*, 2001]. Bank sediments samples were further analyzed for clay mineral identification using an X-ray diffraction technique [*Moore and Reynolds*, 1989]. The X-ray diffraction analysis revealed the presence of a high percentage (>60%) of illite, and a smaller percentage of plagioclase feldspars, and quartz. No smectites were found that could yield an expandable material, susceptible to shear fluid action.

[18] A 241 Am gamma source was used to examine the density distribution and thus homogeneity of the sediment for extracted core samples [*Papanicolaou*, 2001]. The bank sediment composition of Union Flat Creek had homogeneous properties and exhibited fluvial erosion type I [*Papanicolaou*, 2001]. Type I erosion occurs in cohesive sediments that are homogeneous in density and thus the critical erosional strength and other erodibility parameters do not change with depth [*Vermeyen*, 1995]. On the contrary, in fluvial erosion type II, the erodibility parameters are function of depth and time [*Winterwerp and van Kesteren*, 2004].

[19] Lastly, sediment samples were dried and pulverized to measure the median root diameter via an optical scanner-based image analysis [*Costa et al.*, 2001]. Knowledge of the median root diameter and root concentrations atop the sediment surface were deemed important for further evaluation of the erodibility properties [*Thorne*, 1990; *ASCE Task Committee on Hydraulics, Bank Mechanics, and Modeling of River Width Adjustment*, 1998; *Simon and Collison*, 2002; *Gyssels et al.*, 2005; *Pollen and Simon*, 2005, 2006; *De Baets et al.*, 2006].

4.2.2. Erodibility Parameters

[20] The rate of fluvial bank erosion for type I can be quantified using an excess shear stress formula such as [*Kandiah*, 1974]:

$$E = M\left(\frac{\tau_s}{\tau_{cr}} - 1\right)^m \tag{4}$$

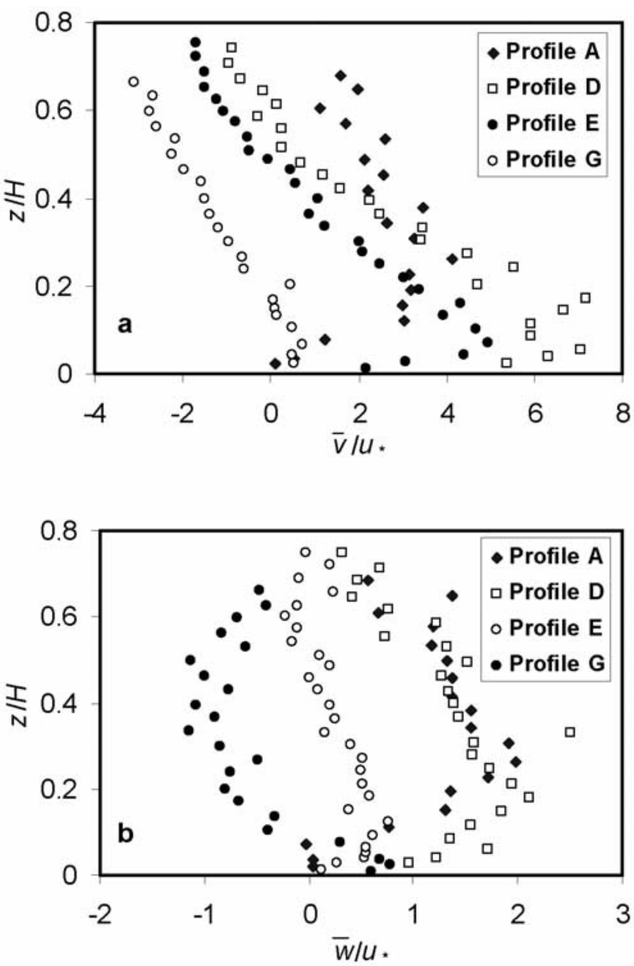

Figure 6. Velocity profiles for locations A, D, E, and G: (a) transverse velocity profiles and (b) vertical velocity profiles.

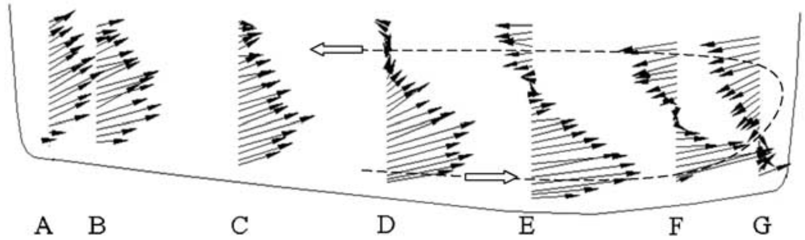

Figure 7. Vector field diagram showing the vertical and transverse velocity vectors, $\sqrt{\overline{v}^2 + \overline{w}^2}$. The counterclockwise circulation is denoted by the dashed line.

where E denotes the fluvial bank erosion rate (Kg/m2/s), M is defined as the erodibility coefficient and has the same units as E, τ_s(Pa), and τ_{cr}(Pa). Similar to τ_{cr}, M also depends upon the sediment properties affecting interparticle forces (e.g., bulk density, sediment composition, organic content, soil age). Both M and τ_{cr} are known in the literature as erodibility parameters and are site specific [*Kandiah*, 1974]. The exponent m is generally considered unity [*Winterwerp and van Kesteren*, 2004]. The steps involved in determining the erodibility parameters are described in a subsequent section.

4.2.3. Laboratory Experiments

[21] Sixty flume runs were performed to determine the erodibility parameters M and τ_{cr} for five undisturbed bank samples extracted from Union Flat Creek. Specifically, twelve runs per sample were conducted for 12 predetermined stress increments.

[22] The erosional strength experiments were performed in a water-recirculating tilting flume that has a useful length of 2.0 m and a width of 0.15 m (Figure 4). The flume was modified to facilitate type I fluvial erosion tests by mounting an easily removable tray (that had a depth of 0.025 m and surface area of 0.02 m^2) atop the flume bed. Undisturbed samples were carved and trimmed to fit the dimensions of the sample tray. The tray was located 82 cm downstream of the entrance (> 30 times the maximum depth considered here), which ensured a developed boundary layer forming atop the sediment sample. The remainder of the flume bed was covered with fine sandpaper to simulate the surface roughness of the sediment (Figure 4). Flow rate was controlled by a gate valve and uniform flow was achieved using an in-stream tailgate.

[23] The flume was set to the proper slope and filled with tap water prior to starting of each experiment. The tap water had a temperature and pH level very close to that of the natural stream water (17°C–18°C and pH of 7.9 compared to 18°C and pH of 8.2 of stream water). As a precursor to testing, a low-flow discharge was supplied to the flume for 10 min to eliminate loose particles from the flume and sample surfaces as a source of error. After that, the flow was adjusted to reach uniform flow.

[24] Eroded sediment was collected just downstream of the sediment sample via four equally spaced 5mm ID glass tubes bent at 90° placed 0.5 cm above the bed of the flume (Figure 4). The incoming flow was judged to have a laterally uniform sediment concentration due to mixing within the flume reservoir. Therefore a single tube was employed upstream of the tray to sample the background concentration. The tubes were discharged into sample bottles simultaneously for 30 s. Approximately 250 mL of water and eroded sediment were collected in each bottle. After collecting the mixture for a specified stress increment, the bottles were replaced by empty bottles and flow was increased to the next predetermined depth/stress increment. The transition to the next stress increment occurred as quickly as possible to minimize unmeasured erosion during the transitional period.

[25] After all stress increments were completed for a given sample, the sediment concentration in each bottle was measured by filtering a 100 mL aliquot through a preweighed and ovendried Whatman 934-AH glass microfiber filter (1.0 μm), which was then oven-dried at 105°C until a constant weight was reached.

[26] The experimental conditions for the runs are given in Table 3. In Table 3, the sediment-eroded value (eleventh column) was taken as the difference between the sediment concentrations measured from the upstream (ninth column) and downstream sampling tubes (tenth column). The erosion rate (twelfth column) was determined by multiplying the flow discharge (column 1) with the sediment-eroded concentration (eleventh column) and dividing by the area of the tray (0.02 m2). For the 60 fluvial erosional runs the error in measuring the concentration column (or erosion column) in Table 3 is less than 9%.

5. Results

[27] In this section, analysis of the field flow measurements collected at the channel expansion are presented first followed by the description of the erodibility results. The flow and fluvial erosion results were linked together to demonstrate the necessary steps for predicting the occurrence of fluvial erosion in channels with transitional planform geometries.

5.1. Flow

5.1.1. Mean and Turbulent Flow Quantities

[28] The distributions of the mean point velocities in the streamwise direction collected in the field for the locations "A"–"G" were plotted against the log law to assess the effects of isolated roughness and possible secondary flows on the primary flow (Figure 5). The points depict the mean point velocities and the solid lines represent the log law [*Kironoto and Graf*, 1994]:

$$\frac{\overline{u}}{u_*} = \frac{1}{\kappa} \ln\left(\frac{z + z_0}{k_s}\right) + B \qquad (5)$$

which was used in the above form to explain the data for both the inner ($z/H < 0.2$) and overlap region ($0.2 < z/H < 0.8$).

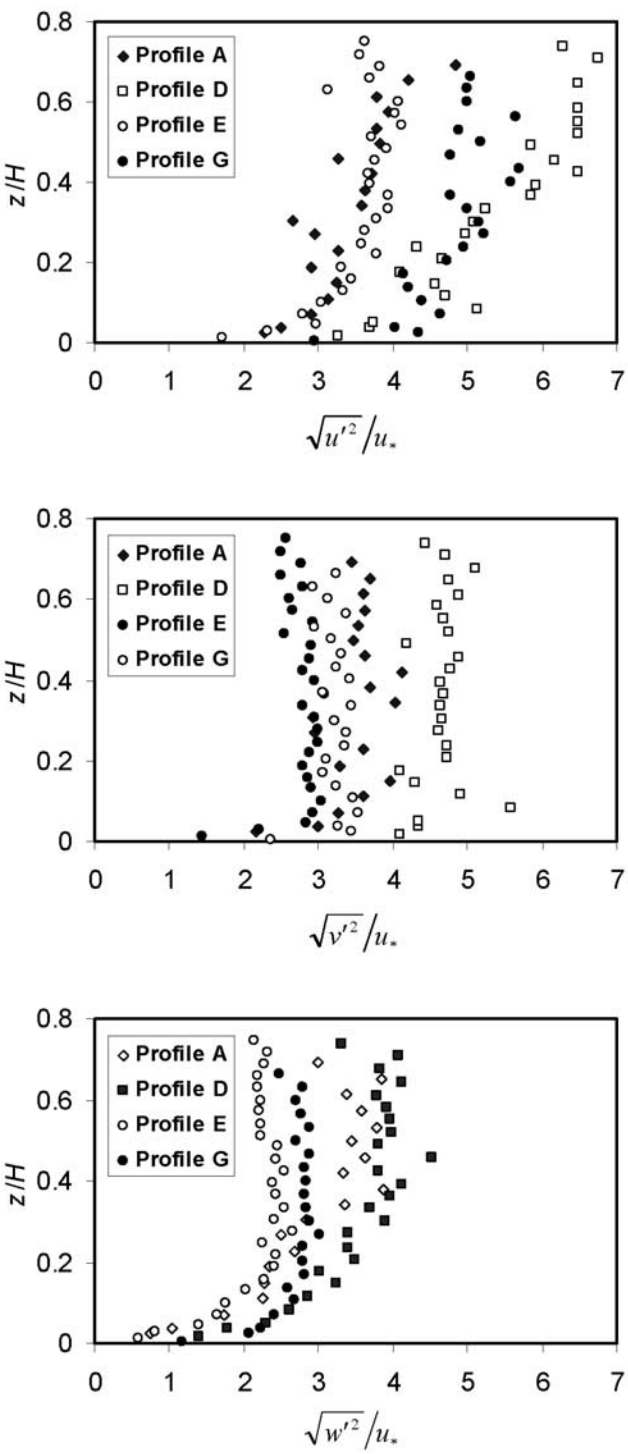

Figure 8. Turbulent intensities for locations A, D, E, and G.

Here, $\bar{u}$ is the mean point velocity (m/s), κ is the von Karman constant, considered to be 0.41, z is the distance above the bed, H is local flow depth, k_s is the roughness scale (taken as d_{50}), z_0 is $0.25k_s$, and B is the constant of integration.

[29] The friction velocity, u_*, and the constant of integration, B, in equation (5) were determined with the method of *Clauser* [1956]. The values of u_* and B are summarized in Table 4. It is important to note that the values of the constant of integration B, (Table 4), differ with those reported in the literature for uniform gravel bed streams, except for the vertical G. For uniform flows in gravel bed streams, *Kironoto and Graf* [1994] reported B = 8.47 ± 0.9 for uniform flows over well packed gravel beds (skimming flow regimes). The smaller B values, reported here, indicate a downward shift, ΔB, of the inner and overlap region of the velocity profile primarily due to greater friction (Figure 5). Table 4 summarizes the ΔB values for all verticals. The largest shift occurred in vertical A while the smallest shift occurred in vertical G. A change in friction is not only a function of the roughness Reynolds number $k^+ = k_s u_*/\nu$ but also of the roughness type (e.g., uniform material versus nonuniform material, mixture of sand and gravel) and the roughness flow regimes (isolated flow, wake interference flow, and skimming flow regime) [*Morris*, 1955; *Schlichting*, 1979; *White*, 1991; *Papanicolaou et al.*, 2001].

[30] While the isolated bed roughness was considered responsible for the systematic deviation of the flow measurements from the log law, the difference found in ΔB values, especially between verticals "A" and "G" (ΔB for A is seven times greater than ΔB for G), was attributed to the complex interaction of secondary flows with the primary flow, and the effects of the plunging flow entering the expansion from the upstream bend [*Knight et al.*, 1984]. As the flow impinged on the left bank (found close to vertical A in Figure 3), the flow became distorted. This distortion introduced an additional retardation to the primary flow at vertical A (in addition to the retardation that was caused by roughness effects). Typically, this retardation is manifested in open channel flows with the presence of a "dip" in the profile of the streamwise velocity below the free surface [*Ead et al.*, 2000]. In the present study, such a "dip" does not appear because no ADV measurements were possible near the free surface. However, the ΔB values shown in Table 4 for all seven profiles clearly indicated that the flow became decelerated, especially for profiles A and B.

[31] The presence of secondary flow is further demonstrated by plotting the distributions of the transverse $\bar{v}$ and vertical $\bar{w}$ point averaged velocities normalized with the friction velocity u_* in Figures 6a and 6b respectively. Because of space limitations only the profiles at the bank verticals A, G and at the centerline verticals D and E were included here. These distributions clearly show that the transverse, normalized velocity vector changes direction (from positive to negative) indicating the presence of a secondary flow (Figure 6a). Similar trends were recorded for the vertical velocity component (Figure 6b).

[32] The vector field of the plane cross-sectional velocity (i.e., the resultant velocity vector of the transverse and vertical velocities $\bar{v}$ and $\bar{w}$ respectively) was plotted in Figure 7 for illustrating the secondary nature of flow. The circulation occurred along verticals D, E, and F in the counterclockwise direction, starting at the bottom of the cross section, thus supporting the notion that secondary flows were present only within the right half of the channel. The flow rotated upward at the right bank in the form of a large-scale secondary current and proceeded into the middle of the channel section and then turned toward the surface. Similar results have been reported by *Nezu et al.* [1993]. *Nezu et al.* [1993] recorded the formation of large-scale free surface secondary currents for flows in streams with comparable width to depth ratios to the one examined here. The

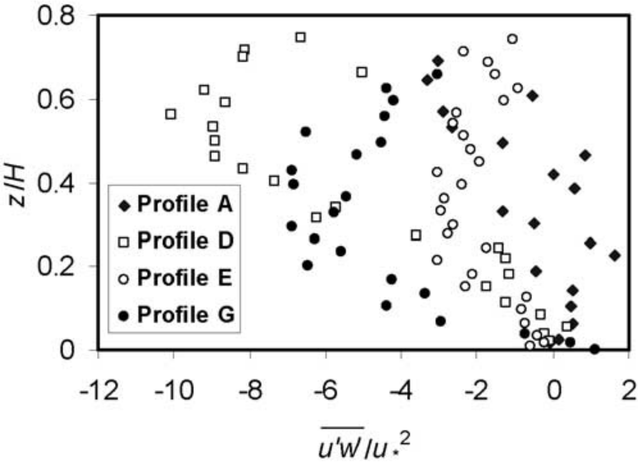

Figure 9. Normalized Reynolds stress in the *x-z* plane ($\overline{u'w'}/u^2$) for profiles A, D, E, and G.

presence of the large current within only the right half of the channel was attributed to the impingement of the flow on left bank.

[33] Maximum turbulent intensities normalized by the friction velocity were encountered near the free surface (Figure 8). The intensity increase with depth, shown in Figure 8, suggested that turbulence momentum was not transferred from the core of the flow to the bed but momentum was transferred from the bed to the free surface which may be attributed to the presence of secondary flows [*Ead et al.*, 2000]. *Mehta* [1981], *Hitoshi et al.* [1995], *El-shewey and Joshi* [1996] and *Xie* [1998] reported similar trends of turbulence intensity increase with depth for flow downstream of a duct or channel transition in the laboratory over smooth walls. The above researchers found that turbulent intensities downstream of an expansion point behave in a manner contrary to conventional findings that report intensity values decreasing toward the free surface. *El-Shewey and Joshi* [1996] attributed this paradoxical behavior to the strong secondary flows developed at the transition point. Along the same lines, *Xie* [1998] showed that cross-sectional irregularity in open channels has the most significant effect on turbulent intensities. The results in Figure 8 support the above discussion by revealing that flow in Union Flat Creek was highly anisotropic, especially along the verticals D, E, and G.

[34] Results for the normalized Reynolds shear stress component $\overline{u'w'}/u_*^2$ in Figure 9 show similar behavior to the intensities. The stress magnitude was greatest in the core of the flow, indicating the presence of a shear layer between the core and free flow surface due to the distortion of the primary flow from the occurrence of secondary currents. Hence production of turbulence occurred at the core of the flow and near the free surface ($z/H \geq 0.2$). Moreover, the nonlinear distribution of the stress indicates the oscillatory nature of the flow induced by the secondary currents [*Nezu and Nakagawa*, 1993].

5.1.2. Sidewall Shear Stress

[35] The sidewall shear stress distribution was calculated using equation (3) for the right bank (near profile G), because this was the side that was affected by the large-scale secondary currents, shown in Figure 7. In equation (3), the terms $\bar{u}\ \bar{w}$ and $\overline{u'w'}$ were determined by fitting lines to the ADV measurements in the transverse and vertical directions. The integration limits in equation (3) were determined as $y_1 = 3.9\ z$ and $y_2 = -3.45\ z$. y_1 describes the bank line geometry of the channel whereas y_2 describes the line separating the channel core flow from the flow contributing to the sidewall shear stress (Figure 3). y_2 was determined by an iterative process by identifying all points at the cross-sectional plane that corresponded to the maximum magnitude of the streamwise velocity.

[36] Because of the secondary flow contributions, the sidewall shear stress (τ_s) obtained values that were 2–5 times greater in magnitude compared to the case that only turbulent contributions were accounted (via the $\overline{u'w'}$ term). Figure 10a compares the distributions of the sidewall shear stress τ_s as a function of z with and without the contributions from secondary currents. The latter distribution of the sidewall shear stress τ_s was constructed by setting $\bar{u}\ \bar{w} = 0$ in equation (3). Because of the highly anisotropic turbulence, both sidewall shear stress distributions departed from a linear distribution. The contributions of the secondary currents were maximized at about 1/4 of the total depth from the channel bottom and were at least twice the magnitude of the average sidewall shear stress, $\bar{\tau}_s$ (Figure 10b). For the 3 July event the maximum τ_s value was 2.83 Pa. Integration of the sidewall shear stress over the bank boundary and dividing by the local water depth H provided an average value of $\bar{\tau}_s = 1.23$ Pa.

[37] To further compare the results provided in this study with other models, the following first-order approximation for the determination of the averaged sidewall shear stresses was considered [*Flintham and Carling*, 1988]:

$$\frac{\bar{\tau}_s}{\rho u_*^2} = SF_{bank}\left(\frac{\left(W_{top} + P_{bed}\right)\sin\theta}{4D}\right) \qquad (6)$$

where θ is the bank angle, W_{top} is the top width of the water surface (m), D is the mean flow depth (m) and SF_{bank} is the proportion of the total shear stress that is acting on the channel banks calculated from $SF_{bank} = 1.77(P_{bed}/P_{bank} + 1.5)^{-1.4}$ in which P_{bed} and P_{bank} are the respective components of the total wetted perimeter (m). The constants used in equation (6) were derived from laboratory data for rectangular and trapezoidal channels. Equation (6) calculates an average sidewall shear stress ($\bar{\tau}_s$) of 0.51 Pa, which is half of the value reported herein (i.e., $\bar{\tau}_s = 1.23$ Pa) and five times less the maximum sidewall shear stress value (i.e., $\bar{\tau}_s = 2.83$ Pa).

[38] Furthermore, the average sidewall shear stress was calculated by the second-order approximation method of *Guo and Julien* [2005],

$$\frac{\bar{\tau}_s}{\rho g D S} = \frac{W}{2D}\left(1 - \frac{4}{\pi}\tan^{-1}\exp\left(\frac{-\pi D}{W}\right) - \frac{\pi D}{W}\exp\left(\frac{-D}{W}\right)\right) \qquad (7)$$

where W is the channel width and D is the mean flow depth. The *Guo and Julien* [2005] value of 1.21 Pa agreed well with the value of 1.23 Pa obtained via our measurements and direct calculations via equation (3).

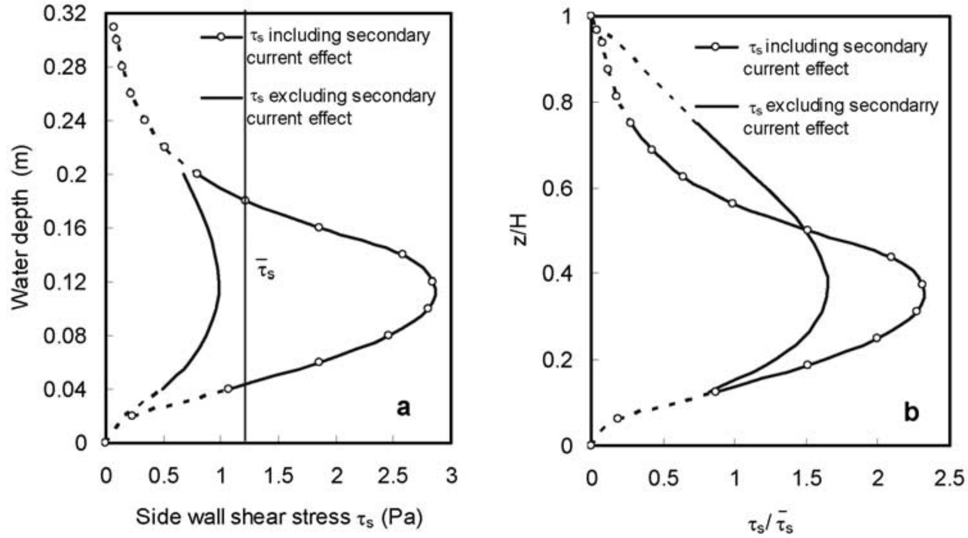

Figure 10. Sidewall shear stress. (a) Sidewall shear stress τ_s as a function of z with and without the contributions from the secondary currents (i.e., the contributions of the $\overline{u}\ \overline{w}$ term in equation (3)). The solid lines represent the measured range of data, while the dashed lines are extrapolated to satisfy the boundary conditions at the streambed and the water surface. The vertical line denotes the average $\overline{\tau}_s$. (b) Normalization of the local sidewall shear stress τ_s over the average $\overline{\tau}_s$ and the corresponding depth z over the local water depth H.

5.2. Erosion Results

5.2.1. Field Observations

[39] A comparison of the bank line prior to and after the 3 July event via the survey measurements showed that no erosion was present. The erosion pin data indicated that no erosion had occurred. The OBS-3 type of measurements provided zero suspended sediment concentration by performing continuous data sampling for a period of 24 h.

[40] Finally, the role of roots found in the extracted bank sediment of Union Flat Creek was assessed. It was found that at the bank toe, root concentration was sparse (i.e., less than 10% of the total exposed surface bank surface area) and the root diameters were very small, i.e., approximately 0.1 mm. It was concluded that vegetation at the bank toe played a rather insignificant role in increasing the value of τ_{cr} for fluvial erosion [*Julian and Torres*, 2006]. This finding was rather qualitative since no direct measurements or calculations were made.

5.2.2. Determination of the Erodibility Parameters

[41] Critical erosional strength was determined by fitting a straight line to the 12 (erosion rates, applied stress) pairs and by extending the line to E = 0 kg/m2/s (Figure 11a). This point was considered to represent the condition when fluvial erosion commenced. The corresponding τ_{cr} was equal to 4.16 Pa. This value was in close agreement with the value of 4.35 Pa reported by *Gilley et al.* [1993] and the measurements of *Mancilla* [2004] who determined a value of 3.6 Pa. In addition, the reported τ_{cr} value was compared with the regression equation of *Julian and Torres* [2006] developed for bank sediments. The *Julian and Torres* [2006] relation provided an average value of 5 ± 2.5 Pa, which was also close to the one reported here.

[42] The value of $M = 1.41 \times 10^{-4}$ kg/m^2/s, which represented the gradient of the fitted line between E and $(\tau/\tau_{cr} - 1)$ in Figure 11b, was comparable to the erodibility values reported in the literature for type I erosion [*Winterwerp and van Kesteren*, 2004]. Typical M values for type I fluvial erosion range between 0.1×10^{-4} kg/m^2/s to 5×10^{-4} kg/m^2/s [*Winterwerp and van Kesteren*, 2004].

6. Discussion

[43] This research addresses the following questions: (1) Is the depth-averaged sidewall shear stress suitable for making bank erosion predictions in channels with pronounced secondary currents? (2) How much additional stress do the secondary currents contribute on the overall magnitude of the depth-averaged sidewall shear stress and local sidewall shear stress? (3) Can laboratory studies be employed, with high confidence, along with field investigations to estimate the erodiblity parameters of sediments?

[44] With respect to question 1, it was found that for transitional channels such as Union Flat Creek, first-order approximations of the averaged sidewall shear stress (such as equation (6)) under predict the fluid shear exerted on the bank perimeter by almost 50%. Second-order approximations (such as equation (7)) may be more suitable for use in transitional channels, however, they are limited to providing information only for the averaged sidewall shear stress and not for the whole sidewall stress distribution. This research showed that τ_s exceeded the $\overline{\tau}_s$ value for almost 50% of the channel depth. This implies that using only the $\overline{\tau}_s$ for making fluvial erosion calculations may lead to an underestimation of the commencement of fluvial bank erosion. In addition, knowledge of the location where $\tau_s(z/H)$ exceeds $\overline{\tau}_s$ may provide unique insight about the areas along the bank perimeter that experience the highest fluid shear action. Field surveys in Union Flat Creek showed that the lower bank section coincided with the areas where cantilevers tend to form. The research presented in this manuscript seems to support therefore the claim made by many

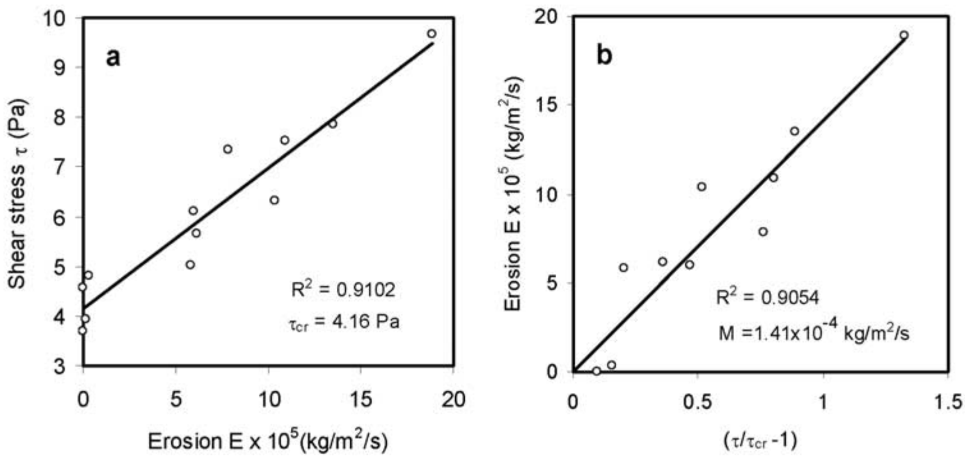

Figure 11. Estimation of sediment erosion parameters from flume experiments: (a) critical erosional strength τ_{cr} and (b) erodibility parameter M. The linear relation between $(\tau/\tau_{cr} - 1)$and E (Figure 11b) suggests that the exponent m in equation (4) is unity for that particular sediment.

researchers [e.g., *Thorne and Tovey*, 1981; *Thorne*, 1990; *Simon et al.*, 1999; *Rinaldi and Darby*, 2005; *Pizzuto et al.*, 2007] that the persistent removal of individual sediment grains from the bank surface due to high shear leads to the formation of cantilevers which in turn promote mass failure.

[45] With respect to question 2, it was found that the presence of secondary currents at least doubled the magnitude of the sidewall shear stress, especially at the lower half of the bank line. Within the lower half of the bank line, the sidewall stress distribution was 2–3 times higher than the Reynolds term in equation (3) (Figure 10a). In addition, secondary currents were found to affect location where turbulence is occurred. Contrary to conventional thinking, it was found that production occurred at the core of the flow and near the free surface ($z/H \geq 0.2$). The nonlinear distribution of the stress indicates the oscillatory nature of the flow induced by the secondary currents.

[46] With respect to question 3, the laboratory experiments (question 3) via the new flume design for determining the erodibility parameters of cohesive bank sediments (erosion type I) provided repeatable results (error less than 9%) which were well compared with those reported in the literature.

[47] The field erosion component of the work reported herein is somewhat limited, however, because data for only one low-flow discharge are reported.

7. Conclusions

[48] By combining detailed field and laboratory tests, this study has put forth a methodology for determining the critical erodibility for fluvial erosion of cohesive banks in streams with pronounced secondary flows. This methodology is expected to be applicable to first and second-order gravel bed streams with homogeneous cohesive bank sediments. Such streams are mostly found in many parts of the world and are characterized by contractions and expansions. These streams have been shown to experience significant secondary currents which in turn exacerbate bank erosion. In particular this study contributes (1) a method for determining the fluid stresses present on the bank by accounting for turbulence and secondary currents, (2) an improved understanding of the turbulence characteristics found in a gradual channel expansion (this was the first detailed report of this nature for natural channels), and (3) a new laboratory procedure for determining the critical erodibility parameters for fluvial erosion type I of cohesive bank sediments.

[49] The findings of this research can be summarized as follows.

[50] 1. Secondary currents generated by channel expansion/contraction affect the turbulent production mode/structure within a channel. We have found that turbulent production downstream of an expansion occurred at the core of the flow and near the free surface. This behavior is contrary to conventional findings that report that turbulent production occurs near channel bed surface.

[51] 2. The measured sidewall shear stress distribution departed from a linear distribution because of the pressure of turbulence anisotropy which was the result of secondary current.

[52] 3. First and second approximation for determining the spatially averaged sidewall stress may not be good predictors of the initiations of bank erosion in channels with expansion/contraction and of similar properties like Union Flat Creek.

[53] 4. The average sidewall shear stress corrected for turbulent and secondary currents obtained a value that was higher than the first-order approximation prediction.

[54] 5. The Union Flat Creek bank sediments exhibited fluvial erosion type I, which may be typical for streams of the Upper Palouse region.

[55] 6. The modified laboratory flume successfully facilitated erodibility tests of fluvial erosion type I. It was found that for the Upper Palouse region and Union Flat Creek, the critical erosional strength for bank sediments obtained a constant value during the summer months. The critical erosional strength value, however, does not remain constant throughout the rest of the year because of diverse subaerial processes.

[56] This research would benefit several types of studies. These include (1) restoration projects in the Pacific North West on small streams experiencing type I bank erosion and (2) bank protection projects. The fact that the sidewall shear stress distribution obtains its maximum value near the bank

toe suggests that stronger bank protection must be provided at the lower part of the bank in order to withstand forces that on average are about 2–4 times the averaged sidewall shear stress.

Notation

C_s concentration of sediment in the water, mg/L.
D mean flow depth, m.
E fluvial bank erosion rate per unit time and unit bank area, kg/m^2/s.
F_r Froude number.
g gravity due to acceleration, m/s^2.
H local flow depth, m.
k_s roughness scale, m.
k^+ roughness Reynolds number.
LL liquid limit.
M erodibility coefficient, kg/m^2/s.
P_{bank} wetted perimeter of the channel banks, m.
P_{bed} wetted perimeter of the channel bed, m.
PL plastic limit.
Q volumetric discharge, m^3/s.
R hydraulic radius, m/s.
R_e Reynolds number.
R_o Rouse number.
S channel slope.
SF_{bank} proportion of the total shear stress that is acting on the channel banks.
SG specific gravity of sediment.
U depth-averaged velocity per profile, m/s.
$\bar{u}$ time average velocities in the streamwise direction x, m/s.
u_* friction velocity, m/s.
V mean velocity, m/s.
$\bar{v}$ time average velocities in the transverse direction y, m/s.
W average channel width, m.
WC_{natural} natural water content, percentage.
$\bar{w}$ time average velocities in the vertical direction z, m/s.
w_s average fall velocity of the sediment particles, m/s.
y_1 lower limit of integration, m.
y_2 upper limit of integration, m.
ϕ friction angle.
γ specific weight of water, N/m^3.
ν kinematic viscosity, m^2/s.
θ bank angle.
ρ fluid density, kg/m^3.
ρ_{bulk} bulk density of sediment, kg/m^3.
τ applied bed shear stress in the flume experiments, Pa.
τ_{cr} critical erosional strength, Pa.
τ_s sidewall shear stress applied by the flow to the bank perimeter, Pa.
$\overline{\tau}_s$ average sidewall shear stress applied by the flow on one bank.
τ_{yx} shear stresses in streamwise direction x applied on the z-x plane, Pa.
τ_{zx} shear stresses in streamwise direction x applied on the y-x plane, Pa.
κ von Karman constant.

[57] **Acknowledgments.** The authors would like to thank the USGS-NIWR program (John Schefter) for funding this project under contract 3995-7941. The comments of J. E. Pizzuto and A. Simon and of the anonymous reviewer have aided in the improvement of the overall manuscript quality. The help/input by Gabriel Mancilla is greatly appreciated. Moreover, the discussion that the first author had with B. C. Yen (University of Illinois at Urbana-Champaign) has helped us to address better the effects of the second kind secondary flows. This paper is dedicated to B. C. Yen's memory for promoting interdisciplinary research in the area of hydraulics/hydrology and sediment transport.

References

Abernethy, B., and I. D. Rutherford (1998), Where along a river's length will vegetation most effectively stabilize stream banks?, *Geomorphology*, *23*, 55–75.
ASCE Task Committee on Hydraulics, Bank Mechanics, and Modeling of River Width Adjustment (1998), River width adjustment. I: Processes and mechanisms, *J. Hydraul. Eng.*, *124*(9), 881–902.
Burt, T. N., and J. R. Stevenson (1983), Field settling velocity of Thames mud, *Tech. Rep. IT-215*, Hydraul. Res. Stn., Wallingford, U. K.
Clauser, F. (1956), The turbulent boundary layer, *Adv.. Appl. Mech.*, *4*, 1–51.
Corbett, D. M. (1962), Stream-gaging procedure, *U. S. Geol. Surv. Water Supply Pap.*, *888*.
Costa, C., L. M. Dwyer, C. Hamel, D. F. Muamba, W. L. Wang, L. Nantais, and D. L. Smith (2001), Root contrast enhancement for measurement with optical scanner-based image analysis, *Can. J. Bot.*, *79*, 23–29.
Couper, P. (2003), Effects of silt-clay content on the susceptibility of river banks to subaerial erosion, *Geomorphology*, *56*, 95–108.
Couper, P. (2004), Space and time in river bank erosion research: A review, *Area*, *36*(4), 387–403.
De Baets, S., J. Poesen, G. Gyssels, and A. Knapen (2006), Effects of grass roots on the erodibility of topsoils during concentrated flow erosion, *Geomorphology*, *76*, 54–67.
Duan, J. G. (2005), Analytical approach to calculate rate of bank-erosion, *J. Hydraul. Eng.*, *131*, 980–990.
Ead, S., N. Rajaratnam, C. Katopodis, and F. Ade (2000), Turbulent open-channel flow in circular corrugated culverts, *J. Hydraul. Eng.*, *26*, 750–757.
El-shewey, I. A., and S. G. Joshi (1996), A study of turbulence characteristics in open channel transitions as a function of Froude and Reynolds numbers using laser technique, in *Advances in Fluid Mechanics*, edited by M. Rahman and C. A. Brebbia, pp. 363–372, Comput. Mech. Publ., Boston, Mass.
Ervine, D. A., and R. H. Sellin (2000), Two-dimensional solution for straight and meandering overbank flows, *J. Hydraul. Eng.*, *126*, 653–669.
Flintham, T. P., and P. A. Carling (1988), The prediction of mean bed and wall boundary shear in uniform and compositely rough channels, in *International Conference on River Regime*, edited by W. R. White, pp. 267–287, John Wiley, Chichester, U. K.
Gilley, J. E., W. J. Elliot, J. M. Laflen, and J. R. Simanton (1993), Critical shear stress and critical flow rates for initiation of rilling, *J. Hydrol.*, *142*(1993), 251–271.
Grissinger, E. H. (1982), Bank-erosion of cohesive materials, in *Gravel-Bed Rivers*, edited by R. D. Hey, J. C. Bathurst, and C. R. Thorne, pp. 273–287, John Wiley, Chichester, U. K.
Guo, J., and P. Y. Julien (2005), Shear stress in smooth rectangular open-channel flows, *J. Hydraul. Eng.*, *131*, 30–36.
Gyssels, G., J. Poesen, E. Bochet, and Y. Li (2005), Impact of plant roots on the resistance of sediments to erosion by water: A review, *Prog. Phys. Geogr.*, *29*(2), 189–217.
Hanson, G. J. (1990), Surface erodibility of earthen channels at high stresses: Part II—Developing an in-situ testing device, *Trans. ASAE*, *33*(1), 132–137.
Hanson, G. J., and A. Simon (2001), Erodibility of cohesive streambeds in the loess area of the midwestern USA, *Hydrol. Processes*, *15*(1), 23–38.
Hitoshi, S., M. Akiyama, P. Mitsunobu, O. Fijita, and T. Sato (1995), Numerical analysis of developing turbulent flow in a square-sectioned 90 degree bend (In Japanese), *Trans. Jpn. Soc. Mech. Eng., Part B*, *61*(587), 2393–2400.
Julian, J. P., and R. Torres (2006), Hydraulic erosion of cohesive river-banks, *Geomorphology*, *76*, 193–206.
Kamphuis, J. W., and K. R. Hall (1983), Cohesive material erosion by unidirectional current, *J. Hydraul. Eng.*, *109*, 49–61.

Kandiah, A. (1974), Fundamental aspects of surface erosion of cohesive soils, Ph.D. thesis, Univ. of Calif., Davis.

Kartha, V. C., and H. J. Leutheusser (1970), Distribution of tractive force in open channels, *J. Hydraul. Eng.*, *96*, 1469–1483.

Kean, J. W., and J. D. Smith (2006a), Form drag in rivers due to small-scale natural topographic features: 1. Regular sequences, *J. Geophys. Res.*, *111*, F04009, doi:10.1029/2006JF000467.

Kean, J. W., and J. D. Smith (2006b), Form drag in rivers due to small-scale natural topographic features: 2. Irregular sequences, *J. Geophys. Res.*, *111*, F04010, doi:10.1029/2006JF000490.

Kironoto, B. A., and W. H. Graf (1994), Turbulence characteristics in rough uniform open-channel flow, *Proc. Inst. Civ. Eng. Water Mar. Energy*, *98*, 118–215.

Knight, D. W., J. D. Demetriou, and M. E. Hamed (1984), Boundary shear in smooth rectangular channels, *J. Hydraul. Eng.*, *110*, 405–422.

Knighton, A. D. (1973), River bank-erosion in relation to streamflow conditions, River Bollin-Dean, Cheshire, *East Midland Geogr.*, *5*(8), 416–426.

Lawler, D. M. (1993), The measurement of river bank-erosion and lateral channel change, *Earth Surf. Processes Landforms*, *18*, 777–821.

Lawler, D. M., C. R. Thorne, and J. M. Hooke (1997), Bank-erosion and instability, in *Applied Fluvial Geomorphology for River Engineering and Management*, edited by C. R. Thorne, R. D. Hey, and M. D. Newson, pp. 137–172, John Wiley, Hoboken, N. J.

Leutheusser, H. J. (1963), Turbulent flow in rectangular ducts, *J. Hydraul. Eng.*, *89*, 1–19.

Mancilla, G. A. (2004), Critical shear stress and rill sediment transport capacity of Palouse soil, Ph.D. thesis, Wash. State Univ., Pullman.

McCool, D., C. Pannkuk, K. Saxton, and P. Kalita (2000), Water runoff and erosion on northwestern USA cropland, *Int. J. Sediment Res.*, *15*(2), 149–161.

Mehta, P. R. (1981), Separated flow through large sudden expansions, *J. Hydraul. Eng.*, *107*, 65–72.

Millar, R. G., and M. C. Quick (1998), Stable width and depth of gravel bed rivers with cohesive banks, *J. Hydraul. Eng.*, *124*, 1005–1013.

Moore, D. M., and R. C. Reynolds (1989), *X-Ray Diffraction and the Identification and Analysis of Clay Minerals*, 332 pp., Oxford Univ. Press, New York.

Morris, H. (1955), Flow in rough conditions, *Trans. Am. Soc. Civ. Eng.*, *120*, 373–398.

Nezu, I., and H. Nakagawa (1993), *Turbulence in Open Channel Flows*, A. A. Balkema, Rotterdam, Netherlands.

Nezu, I., A. Tominaga, and H. Nakagawa (1993), Field measurements of secondary currents in straight rivers, *J. Hydraul. Eng.*, *119*, 598–614.

Northwest Power Planning Council (2001), Palouse subbasin summary, Portland, Oreg.

Papanicolaou, A. N. (2001), Erosion of cohesive streambeds and banks, *State Wash. Water Res. Cent. Rep. WRR-08*, Wash. State Univ., Pullman, Wash.

Papanicolaou, A. N., P. Diplas, C. Dancey, and M. Balakrishnan (2001), Surface roughness effects in near-bed turbulence: Implications to sediment entrainment, *J. Eng. Mech.*, *127*(3), 200–218.

Pizzuto, J. E., and the ASCE Task Committee on Hydraulics, Bank Mechanics, and Modeling of River Width Adjustment (2007), Streambank-erosion and river width adjustment, *ASCE 110 Sedimentation Manual*, Am. Soc. of Civ. Eng., Reston, Va., in press.

Pollen, N., and A. Simon (2005), Estimating the mechanical effects of riparian vegetation on stream bank stability using a fiber bundle model, *Water Resour. Res.*, *41*, W07025, doi:10.1029/2004WR003801.

Pollen, N., and A. Simon (2006), Temporal and spatial variability in the root-reinforcement of streambanks: Incorporating variations in soil shear strength and soil moisture into the rip root model, in *Proceedings of the 2006 World Environmental and Water Resources Congress*, edited by R. Graham, pp. 87–91, John Wiley, Hoboken, N. J.

Rinaldi, M., and S. E. Darby (2005), Advances in modeling river bank-erosion processes, paper presented at 6th International Conference on Gravel-Bed Rivers, AGU, Vienna, Austria.

Schlichting, H. (1979), *Boundary Layer Theory*, 7th ed., McGraw-Hill, New York.

Simon, A., and A. Collison (2002), Quantifying the mechanical and hydrologic effects of riparian vegetation on streambank stability, *Earth Surf. Processes Landforms*, *27*, 527–546.

Simon, A., and M. Rinaldi (2000), Channel instabilities in the loess area of the Midwestern United States, *J. Am. Water Resour. Assoc.*, *36*(1), 1–18.

Simon, A., A. Curini, S. E. Darby, and E. J. Langendoen (1999), Streambank mechanics and the role of bank and near-bank processes in incised channels, *Incised River Channels: Processes, Forms, Engineering, and Management*, edited by S. E. Darby and A. Simon, pp. 123–152, John Wiley, London.

Simon, A., A. Curini, S. E. Darby, and E. J. Langendoen (2000), Bank and near-bank processes in an incised channel, *Geomorphology*, *35*, 193–217.

Simons, D. B., and F. Senturk (1992), *Sediment Transport Technology: Water and Sediment Dynamics*, 2nd ed., Water Resour. Publ., Littleton, Colo.

Thorne, C. R. (1982), Processes and mechanisms of river bank-erosion, in *Gravel-Bed Rivers*, edited by R. D. Hey, J. C. Bathurst, and C. R. Thorne, pp. 227–271, John Wiley, Chichester, U. K.

Thorne, C. R. (1990), Effects of vegetation on riverbank-erosion and stability, in *Vegetation and Erosion*, edited by J. B. Thornes, pp. 125–144, John Wiley, Hoboken, N. J.

Thorne, C. R., and N. K. Tovey (1981), Stability of composite river banks, *Earth Surf. Processes Landforms*, *6*, 469–484.

White, F. M. (1991), *Viscous Fluid Flow*, 2nd ed., McGraw-Hill, New York.

Winterwerp, J. C., and W. M. van Kesteren (2004), *Introduction to the Physics of Cohesive Sediment in the Marine Environment*, *Dev. Sedimentol.*, vol. 56, edited by J. C. Winterwerp and W. G.M. van Kesteren, Elsevier, Amsterdam.

van Prooijen, B. C., J. A. Battjes, and W. J. Uijttewaal (2005), Momentum exchange in straight uniform compound channel flow, *J. Hydraul. Eng.*, *131*, 175–185.

Vermeyen, T. (1995), Erosional and depositional characteristics of cohesive sediments found in Elephant Butte Reservoir, New Mexico, *Tech. Rep. R-95-15*, Bur. of Reclam., Denver, Colo.

Xie, Q. (1998), Turbulent flows in non-uniform open channels: Experimental measurements and numerical modeling, Ph.D. thesis, Univ. of Queensland, Queensland, Brisbane, Australia.

M. Elhakeem and A. N. Papanicolaou, Department of Civil and Environmental Engineering, IIHR-Hydroscience and Engineering, University of Iowa, Iowa City, IA 52242, USA. (apapanic@engineering.uiowa.edu)

R. Hilldale, Sedimentation and River Hydraulics Group, Technical Service Center, Bureau of Reclamation, P.O. Box 250007, Denver, CO 80225, USA.